Ecofriendly Production of CuO/ZnO Nanocomposites from Guava Leaf Biomass and their Antimicrobial and Selective Anticancer Activities

Sulaiman A. Alsalamah [a,*] Mohamed M. Alawlaqi [b] Mari Sumayli [b] Sultan Mohammed Areshi [b] Yehia Hazzazi [b] Mohammed Ibrahim Alghonaim [a] and Abdullah M. Almotayri [c]

Psidium guajava leaf extract was utilized to produce CuO NPs and CuO/ZnO nanocomposites in this work. X-ray diffraction patterns showed the proper phase of the synthesized sample, and using Scherrer's equation, the mean crystallite sizes were calculated to be 13.05 nm and 13.07 nm for CuO nanoparticles (NPs) and CuO/ZnO nanocomposite, respectively. From transmission electron microscopy images and particle size distribution from ImageJ, the samples had larger sizes of 84.6 nm and 96.6 nm, respectively. Fourier transform infrared (FTIR) spectroscopy also indicated the successful fabrication of the CuO NPs and CuO/ZnO nanocomposite, as the IR spectrum showed peaks at 611 and 521 cm^{-1} for Cu–O and Zn–O, respectively. The biological activities were found to be higher for the CuO/ZnO nanocomposite than the CuO NPs alone. The inhibition zones recorded were 28 mm and 25 mm for *Bacillus. subtilis* and *Staphylococcus aureus*, respectively, followed by 24 mm and 21 mm for *Salmonella typhi* and *Klebsiella pneumoniae*, respectively. The nanocomposite exhibited selective cytotoxicity properties because the IC_{50} values for Wi38 (normal human fibroblast cells) and SKOV3 (human ovarian carcinoma cells) were 295.48 and 81.87 µg/mL, respectively. Antioxidant analysis of (2,2-diphenyl-1-picrylhydrazyl) (DPPH) radical scavenging activity was found to be 6.93 µg/mL for the nanocomposite

DOI: 10.15376/biores.21.2.2906-2924

Keywords: CuO/ZnO nanocomposites; Antimicrobial activity; Antioxidant; Cytotoxicity

Contact information: a: Department of Biology, College of Science, Imam Mohammad Ibn Saud Islamic University (IMSIU), Riyadh 11623, Saudi Arabia; b: Department of Biology, College of Science, Jazan University, P.O. Box 114, Jazan 45142, Saudi Arabia;c: Department of Biology, Faculty of Science, Al-Baha University, 65779 Al-Baha, Saudi Arabia;
** Corresponding author: SAAlsalamah@imamu.edu.sa*

INTRODUCTION

Nanotechnological approaches have increasingly been applied in agricultural and medical fields (Abdelghany *et al.* 2023a; El-Batal *et al.* 2023; Amin *et al.* 2025). The concept of "green" production of nanoparticles (NPs) by means of plant mediators has become a preferred strategy in an attempt to avoid the ecological and economical toxicity involved in the chemical synthesis (Alghonaim *et al.* 2025; Selim *et al.* 2025a). The physical property of NP size with high surface-area-to-volume ratios results in an unmatched catalytic, optical, and reactive potential. Polymer, lipid, or metal- or metal

oxide-based NPs have therefore been applied for energy storage, remediation, and medicinal uses, particularly for imaging or drug delivery (Abdelghany *et al.* 2018). Copper (II) oxide (CuO) NPs, for instance, exhibit strong antioxidant, antimicrobial, and anticancer potential (Abdelghany *et al.* 2020; Alsalamah *et al.* 2025). The subcellular size of NPs allows for targeted cellular uptake, which can offer improved results with minimal systemic damage to the host organism. Additionally, scientists have developed NP nanocomposites to offer even more selectivity for regenerative and cancerous therapies.

Similarly to CuO, Zn oxide-containing NPs have shown great potential due to the unique way that they behave biologically. Zn oxide-containing NPs function as a selective cytotoxic agent against MCF7 that produce reactive oxygen species (ROS) for a cascade of effects that eradicate cancer cells and microbes while sparing healthy cells of the Vero cell line CCL-81 (Qanash *et al.* 2024). The potential of Zn oxide-containing NPs also extends to agricultural applications as a nano-fertilizer to improve crop growth (Abdelghany *et al.* 2023b, 2024), to the food industry as a shelf-life preservative through antimicrobial packaging, and finally to cosmetic applications as well due to its photocatalytic and UV-shielding properties.

Composites of two metals or metal oxides combine the unique properties of each component to achieve enhanced functionality compared to single-phase nanoparticles (Al Abboud *et al.* 2024). In such biphasic metal or metal oxide nanocomposites, interactions between the two phases can improve its stability, reduce agglomeration, and induce biological activity (Selim *et al.* 2025b). For example, combining CuO and ZnO into a single nanocomposite can merge the potent biological properties of CuO with the biocompatibility and ROS-mediated activity of ZnO (Al-Rajhi *et al.* 2022). Additionally, the structural and electronic interactions in biphasic composites can enhance surface reactivity, facilitating improved cellular uptake, ROS generation, and overall therapeutic performance. Here, the term "biphasic" means that methods such as X-ray diffraction (XRD) will reveal two distinct phases. Such nanocomposites have broad applications in biomedicine, catalysis, and environmental remediation, making them a promising platform for multifunctional nanoscale materials (Das and Srivastava 2018).

Scientists think that green-synthesised NPs are safer to work with than chemically produced ones (Nguyen *et al.* 2018). In this study, the authors used guava (*Psidium guajava*) leaves extract as capping agent to create CuO and CuO/ZnO NPs. This plant is found in tropical and subtropical areas. Numerous physiological compounds with antioxidative and anti-inflammatory properties, including flavonoids, triterpenoids, alkaloids, and tannins, are found in high concentrations in its leaves (Park *et al.* 2024).

Plant extracts appear to serve as a mediator in the green synthesis of ZnO NPs. In contrast to noble metal NPs, where reduction of metal ions is essential, ZnO formation does not involve a change in oxidation state, as zinc exists in the +2 oxidation state both in zinc acetate precursors (for example) and in the final ZnO lattice (López-López *et al*. 2021). In this context, the role of extracts is not a redox-driven reduction but rather the promotion of Zn^{2+} hydrolysis, condensation, and controlled nucleation, leading to formation of ZnO (Hamed *et al*. 2023). Phytoconstituents act as complexing and chelating agents that regulate Zn^{2+} speciation, enable the formation of $Zn(OH)_2$ intermediates, and subsequently direct their dehydration into ZnO. Additionally, these biomolecules serve as stabilizing and capping agents, preventing NPs agglomeration and controlling morphology and particle size. Similar non-redox mechanisms have been extensively reported for the biosynthesis of ZnO NPs. While in some other cases, plant extracts have been shown to act as reducing

agents, they appear to have a broader role in NPs formation rather than causing a change in zinc's valence state (Matinise *et al.* 2017). Little is known about the multifunctional use of CuO/ZnO NPs compared with monophasic CuO NPs. Thus, this study established a comparison of monophasic and biphasic oxide NPs as biological agents in different pharmacological and medical uses.

EXPERIMENTAL

Extracting Plant Extract

Psidium guajava leaves were collected from the Botanical Garden of Al-Qanater El-Khyria (El-Qulyubia Governorate, Egypt). The collected plant biomass was rinsed with distilled deionized water and air-dried under room temperature in the shade for five days. Five grams of the plant powder were suspended in 100 mL double-distilled deionized water and heated at 70 °C for 20 min. The decoction was filtered through Whatman No. 1 filter paper, and the filtrate was kept at 4 °C for further use.

Preparation of CuO/ZnO Nanocomposites and CuO NPs

For combined-phase CuO/ZnO nanoparticles, 50 mL each of 0.5 M copper sulfate and 0.5 M of zinc acetate was mixed to form the precursor solution. The mixture was heated at 80 °C with magnetic stirring. 50 ml of leaves extract was added dropwise after reaching the desired temperature. The synthesis reaction was allowed to proceed for 50 min. The resultant precipitate was separated through centrifugation (4800 rpm, 15 min) and calcined at 450 °C for 3 h. The CuO nanoparticles were synthesized using the identical thermal and mechanical protocol using copper sulfate alone.

Characterization of Synthesized CuO/ZnO Nanocomposites and CuO NPs

The synthesized particles were characterized structurally and chemically. Fourier transform infrared by FTIR (Thermo Scientific Nicolet iS50 FT-IR spectrometer) spectroscopy was used to recognize the functional groups present during the synthesis. The Shimadzu XRD-6000 lists, SSI, (Japan) was used to determine the crystallinity of the CuO/ZnO Nanocomposites and CuO NPs. The Scherrer equations were used to measure the diameters of the nanoparticles. The average crystallite size of the biosynthesized NPs was determined using the Scherer equation ($D = 0.9\ \lambda/\beta\ \cos\theta$) to estimate the particle size of NPs. Next, *d*-spacing ($dhkl = \lambda/(2\sin\ \theta)$, micro-strain ($\varepsilon = \beta/4\tan\ \theta$), and dislocation density ($\delta = 1/D\text{^}2$) were computed (Table 1).

Transmission electron microscopy (TEM) images were obtained using a JEM-2100 PLUS electron microscope (JEOL, Japan) running at 200 kV with a LaB6 source. The energy dispersive X-ray spectroscopy (EDX) investigation of these samples was performed using a JEM-2100 F (URP) device equipped with a Dry SD30GV detector and set at 200 kV.

Antimicrobial Assay (Agar Well Diffusion Method) of CuO/ZnO Nanocomposites and CuO NPs

The agar well diffusion method (Qanash *et al.* 2023) was employed to determine the antimicrobial activities of the as-synthesized CuO and CuO/ZnO nanocomposites. The test panel included four bacterial isolates: *Staphylococcus aureus* (ATCC 6538), *Bacillus*

subtilis (ATCC 6633), *Klebsiella pneumoniae* (ATCC 13883), and *Salmonella typhi* (ATCC 6539), as well as two fungal isolates: *Candida albicans* (ATCC 10221) and *Aspergillus terreus* (ATCC 20542). The inoculum was prepared by standardizing the turbidity of bacterial and fungal cultures to 0.5 McFarland turbidity standard. The medium was swabbed with the standardized inoculum to form confluent growth on sterile Mueller–Hinton agar (MH agar) plates (bacteria) or Sabouraud dextrose agar plates (fungi). After punching 6-mm wells in the media, 100 µL of each nanoparticle dispersion was added to the respective wells. Dimethyl sulfoxide (DMSO) was used as a control and Gentamicin (10 µg/mL) or Fluconazole (25 µg/mL) was used as the positive standard in the antibacterial or antifungal assay, respectively. A 30-minute pre-incubation step was added to allow the test compounds to diffuse, followed by separate incubation conditions for bacterial plates (37 °C for 24 h) and fungal plates (28 to 30 °C for 48 to 72 h), after which antimicrobial activity was measured using a digital caliper to measure the diameter of the zone of inhibition (ZOI) in millimeters.

Cytotoxicity Assay (MTT Assay) of CuO/ZnO Nanocomposites and CuO NPs

The cytotoxicity studies were performed on two cell lines: SKOV3 human ovarian carcinoma (ATCC® HTB-77™) and Wi38 normal human fibroblasts (ATCC® CCL-75™). Cell cultures were maintained at 37 °C with 5% CO_2 in a humidified incubator and in Dulbecco's Modified Eagle Medium (DMEM) supplemented with 10% fetal bovine serum (FBS) and 1% penicillin–streptomycin. After seeding the cells (1×10^4 cells/well in 96-well plates) and incubating for 24 h for cell attachment, the samples were treated with the CuO or CuO/ZnO nanoparticles in a concentration range of 31.25 to 1000 µg/mL for 24 h. The metabolic activity of the cells was measured by MTT assay. To each well, 20 µL of MTT reagent (5 mg/mL) was added and incubated for 4 h. After solubilization of the formazan crystals with 150 µL DMSO, the absorbance was measured at 570 nm. The changes in the cell morphology were also observed with an inverted phase-contrast microscope and the cell viability was calculated using the standard formula:

$$\text{Cell viability (\%)} = \frac{\text{Absorbance of treated cells}}{\text{Absorbance of control cells}} \times 100 \quad (1)$$

From this, the cytotoxicity (%) can be derived as:

$$\text{Cytotoxicity (\%)} = 100 - \text{Cell viability (\%)} \quad (2)$$

DPPH Radical Scavenging Assay of CuO/ZnO Nanocomposites and CuO NPs

Radical scavenging activity was determined using the DPPH method. Aqueous suspensions of equal volumes (1 mL) of nanoparticle solution and 0.1 mM methanolic DPPH were mixed and kept at room temperature in the dark for 30 min. The absorbance of the mixture was measured at 517 nm (Alawlaqi *et al.* 2023). The scavenging efficiency was calculated using Eq. 1,

$$\text{Scavenging activity (\%)} = \frac{A_{\text{control}} - A_{\text{sample}}}{A_{\text{control}}} \times 100 \quad (3)$$

where A_{control} is the absorbance of the DPPH solution without sample, and A_{sample} is the absorbance of the tested sample. The concentration of each tested compound required to scavenge 50% of DPPH radicals (IC_{50}) was determined by plotting the percentage

scavenging activity against the compound concentration and fitting a suitable regression curve.

Statistical Analysis

Data processing was performed using SPSS software (version 18, IBM Corp., Armonk, NY, USA). The statistical framework included One-Way analysis of variance (ANOVA), Shapiro-Wilk normality tests, and Homogeneity of Variance checks, supplemented by appropriate *post-hoc* comparisons and evaluated honest significant differences (HSD).

RESULTS AND DISCUSSION

Characterization of CuO and CuO/ZnO NPs

A limitation in the use of vegetal matrices in the biosynthesis of nanoparticles is the question of its mechanistic predictability, due to the complexity of the plant extract. Although the exact mechanism of various phytochemical interactions in this process is not fully understood yet, the reduction and stabilization of NPs is mainly due to the reductant action of some specific bioactive moieties, such as carbonyl, hydroxyl, and methoxide groups, all of which are richly available in plant metabolites, such as phenolic compounds, flavonoids, alkaloids, and proteins (Devi *et al.* 2016; Abd-ElGawad *et al.* 2025). To make a correlation between this chemical scenario and the physico-structural one, the synthesized monophasic (CuO) and biphasic (CuO/ZnO) species were characterized using TEM and EDX (Amin *et al.* 2024, 2025). The morphometric analysis with ImageJ software recorded a wide range of particle sizes (67.9 to 122.07 nm) (Fig. 1a, b). The calculated average particle size was also different for pure CuO and CuO/ZnO, *i.e.*, 84.63 and 96.6 nm, respectively (Fig. 1c, d). The particles exhibited semi-spherical and irregular shapes (Fig. 1a,b). The morphology was not entirely consistent with the results from Cao *et al.* (2021) (semi-spherical CuO/ZnO-doped nanoparticles with size in the range of 20 to 130 nm). They observed spherical shapes only. In contrast, some simultaneous reports point that the one-phasic composites (either CuO or ZnO) usually have similar and small diameters.

After the preparation of the biphasic CuO/ZnO nanoparticles, their propensity to agglomerate was observed. This issue is one of the common reasons for the biphasic NPs' aggregation as the van der Waals attractive forces are stronger than their repulsive ones. The most significant feature is that, according to Turabik *et al.* (2023), although the morphological characteristics of mono- and biphasic particles are essential, their functionality and versatility are primarily defined by the surface-related physicochemical parameters such as zeta potential, pore width, or specific surface area. Energy dispersive X-ray spectroscopy was also applied to ensure the presence of targeted elements (Fig. 2a,b).

The spectrum corresponding to monophasic CuO nanoparticles shows the most intense peaks corresponding to the Copper (Cu) and Oxygen (O). As for the carbon (C) signals, they are probably related to the plant extract-based biomolecules acting as capping agents to stabilize the NPs. The EDX spectrum of the prepared biphasic CuO/ZnO nanocomposites resolved the peaks of all target elements – copper, zinc, and oxygen. Carbon signals were also detected, which could also be assigned to the organic compounds that stabilized the nanostructures.

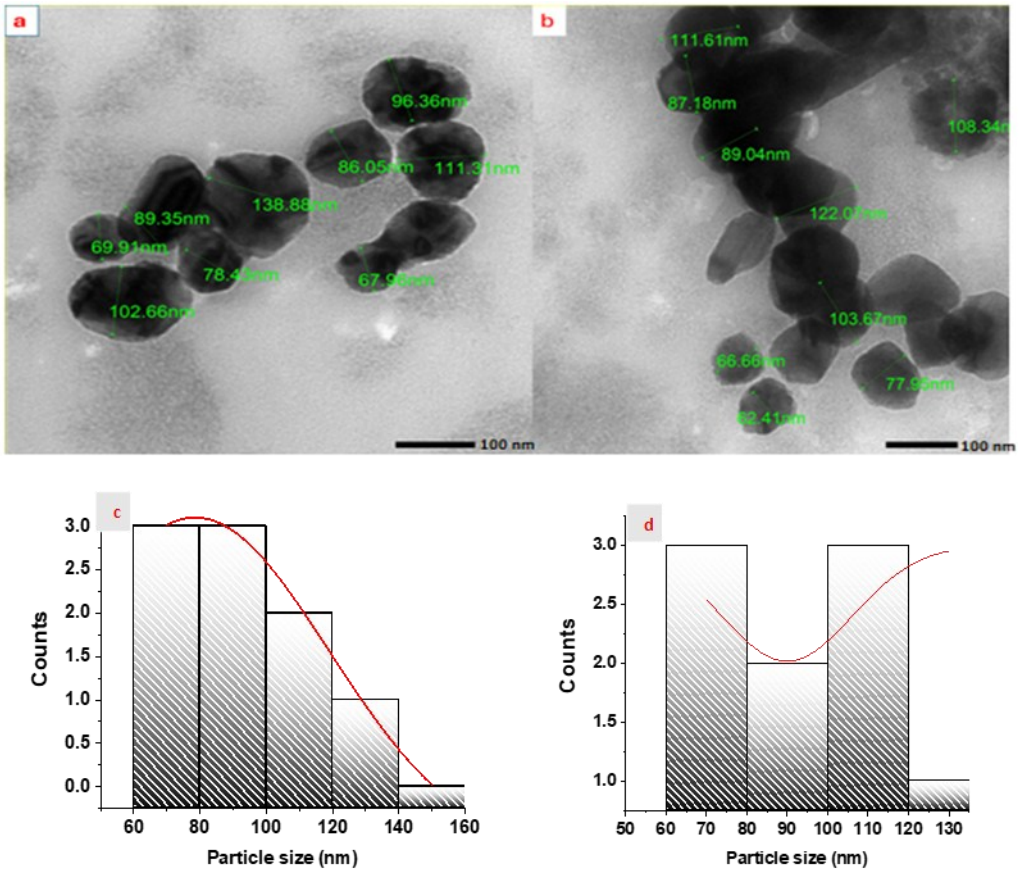

Fig. 1. TEM images (a, b) of CuO and CuO/ZnO NPs, respectively

To investigate the vibration properties of the biosynthesized samples and to confirm the identity of the *Psidium guajava* metabolites involved in capping and stabilization, FTIR spectroscopy was used (Fig. 3). The broad absorption bands present at 3473 cm^{-1} and 3454 cm^{-1} in the higher frequency region are assigned to the stretching vibrations of hydroxyl (-OH) groups and are possibly due to surface-adsorbed water molecules. The adsorption of atmospheric CO_2 is confirmed by the presence of a distinct peak at 2,355 cm^{-1} (Senthilkumaar *et al.* 2008). The peak centered at around 1630 cm^{-1} due to the C=O stretching mode of carboxylic acid moieties is a clear indicator of the role of these functional groups in the reduction process (Atiek *et al.* 2024). The bands present at 1400, 1413, and 1220 cm^{-1} are assigned to the vibrations of aromatic rings and C–C/C–OH stretching of polyol compounds. These observations further validate that the bioactive organic ligands present in the leaf extract are adsorbed on the nanoparticle surface and contribute to the steric stability.

The formation of the inorganic core is evident from vibrations in the low frequency fingerprint region. The formation of copper oxide is confirmed by the Cu–O stretching vibrations centered at 610 cm^{-1}, 611, and 680 cm^{-1} (Vishveshvar *et al.* 2018). The Zn–O stretching vibration is associated with the peak found at 423 cm^{-1}, confirming the ZnO production (Music *et al*. 2002). As confirmed by the associated EDX profile (Fig. 2), these spectral analyses reconfirmed that Cu, Zn, and O were the major elements present in the samples.

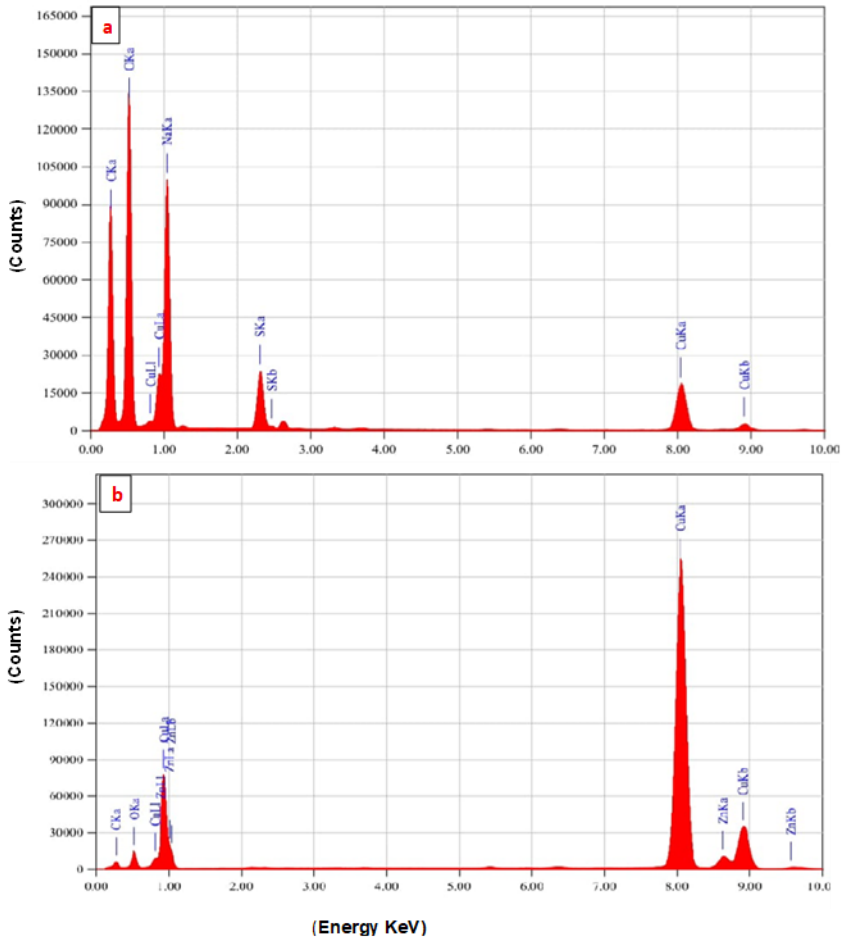

Fig. 2. EDX analysis (a, b) of CuO and CuO/ZnO NPs, respectively

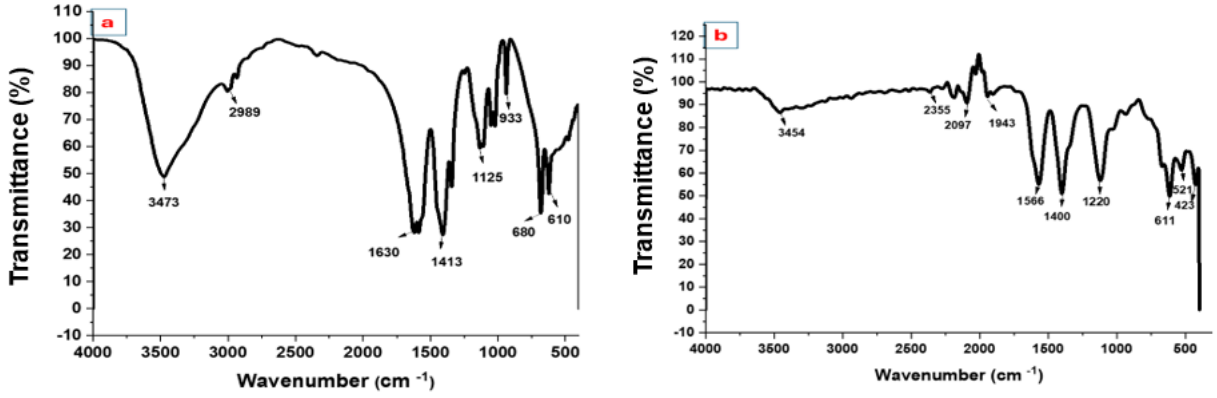

Fig. 3. FTIR analysis of a) CuO and b) CuO/ZnO NPs

The XRD analysis was used to determine whether the produced nanocomposite was crystalline or amorphous. The successful doping and development of crystallographic CuO NPs and CuO/ZnO nanocomposite is indicated by the appearance of sharp and distinct peaks for Cu and Zn in the XRD analysis (Fig. 4). The XRD pattern of the CuO NPs is displayed in Fig. 3. Monoclinic CuO's (111), (200), (220), and (311) planes are responsible

for the peaks that were seen at 43.40°, 50.55°, 74. 30°, and 90.16° (COD Reference: 9012954 and 1509146). Additionally, the highest points found at 36.29°, 39, 54.33, and 70.04 were in accordance with the (002), (101), (110), and (103) planes of hexagonal ZnO, respectively (COD Reference: 9008781). The crystalline structure of copper oxide nanoparticles is demonstrated by their strong reflection and well-defined appearance in XRD patterns (Bashiri Rezaie *et al.* 2018). Their crystalline structure is revealed by the XRD spectrum's strong peaks (Yallappa *et al.* 2013).

The Scherrer formula was used to determine the average crystallite sizes of CuO and CuO/ZnO nanoparticles and were found to have average crystallite diameters of 13.05 and 13.07 nm, respectively. Table 1 shows the different properties of XRD spectrum, which appeared in CuO and CuO/ZnO NPs. Increased dislocation density causes lattice distortions, leading to increased micro-strain, which in turn subtly alters the ideal d-spacing (interplanar distance) observed in XRD, often showing a slight decrease or shift from standard values, with composites showing complex interplay between CuO and ZnO properties. Higher strain/dislocations typically correlate with smaller crystallite sizes and *vice versa*, with CuO/ZnO composites often exhibiting modulated properties compared to pure phases due to heterojunctions and doping effects.

Table 1. XRD Parameters for CuO and CuO/ZnO NPs

2θ (°)	FWHM (β)	Size (nm)	Dislocation Density (ρ) nm^{-2}	micro-strain (ε) 1μ/m	d-spacing
	CuO				
43.40	0.755	11.31	7.80	8.28	1.120
50.55	0.752	11.68	7.32	6.94	0.997
74.30	0.725	13.73	5.29	4.17	0.800
90.16	0.727	15.46	4.17	3.16	0.770
Average	0.740	13.05	6.15	5.64	0.922
CuO/ZnO NPs					
36.29	0.704	11.86	7.10	9.38	1.30
39.00	0.707	11.90	7.05	8.72	1.22
43.28	0.709	12.04	6.89	7.80	1.12
50.43	0.705	12.45	6.44	6.53	0.99
54.33	0.708	12.59	6.30	6.02	0.94
70.04	0.708	13.69	5.33	4.41	0.81
74.12	0.706	14.09	5.03	4.08	0.80
89.93	0.704	15.93	3.93	3.07	0.77
Average	0.706	13.07	6.01	6.25	0.99

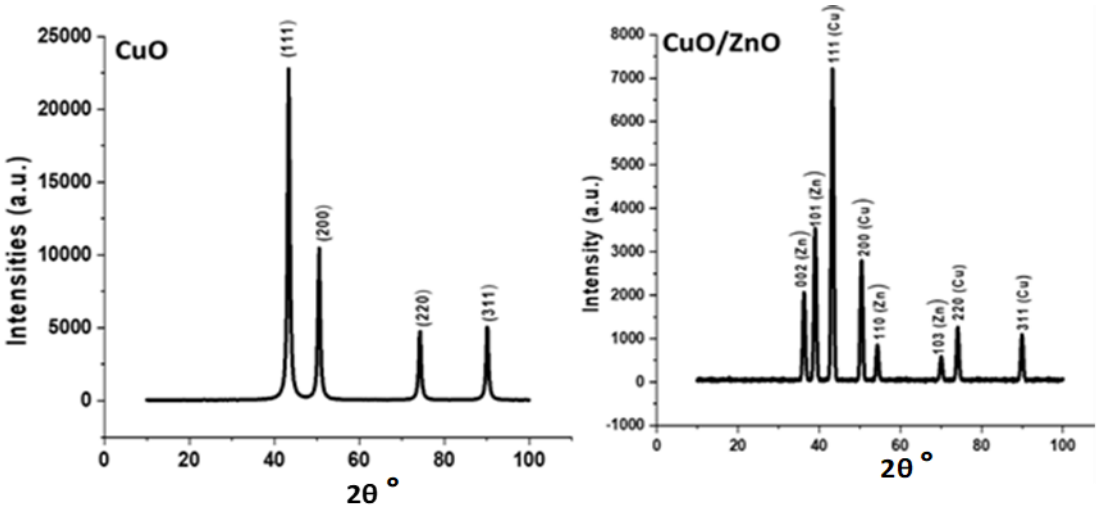

Fig. 4. XRD analysis CuO and CuO/ZnO NPs

Biological Potential

Table 2 indicates that the antibacterial activity of the CuO/ZnO nanocomposite was improved when compared with CuO nanoparticles and the negative controls. Statistically, the CuO/ZnO nanocomposite showed highly significant increases of inhibition zones of pathogenic microorganisms. Of the six different tested microorganisms (two fungal strains and four bacterial strains), *B. subtilis* (Gram-positive) was the most sensitive. Zone of inhibition was 28 ± 0.1 mm for *B. subtilis* and 25 ± 0.1 mm for *S. aureus*, which may indicate that the nanocomposite penetrated the relatively thicker peptidoglycan layer in Gram-positive bacterial strains. For the Gram-negative strains, *S. typhi* and *K. pneumoniae* showed 24 ± 0.2 mm and 21 ± 0.2 mm zones of inhibition, respectively, even though they have stronger outer membrane layers compared to Gram-positive strains. The improved action against Gram-negative bacteria suggests that the biphasic CuO/ZnO composition was effective to disrupts membrane integrity and interferes with essential metabolic processes. The plates (Fig. 5) visually confirm the quantitative data, showing larger, clearer inhibition halos around the CuO/ZnO wells for all bacteria tested. Across all bacterial plates, the negative control produced no inhibition, validating the experiment, while the positive control showed moderate, consistent activity. The superior inhibition halos around the CuO/ZnO wells visually document the enhanced antibacterial potency and the combination effect of the composite nanoparticles. The enhanced bactericidal effect was attributed to the combined antibacterial effects from the copper and zinc oxide phases. This is mainly due to the catalytic generation of ROS as a possible mechanism based on previously reported literature (Fani *et al*. 2025; Ma *et al.* 2025), such as hydrogen peroxide, superoxide ions, and hydroxyl radicals, that cause oxidative damage to DNA, proteins, and lipids. At the same time, the dissolution of Cu^{2+} and Zn^{2+} enabled intracellular entry, which interfered with enzyme activity and metabolic balance. The physicochemical characteristics with a high surface area and strong electrostatic attraction enabled the nanohybrids to attach firmly to the bacterial surface. It destabilizes the dense peptidoglycan layer of Gram-positive bacteria and disrupts the recalcitrant outer membrane of Gram-negative bacteria, causing substantial changes in permeability and cytoplasmic leakage. Overall, the dual-phase system creates multiple simultaneous attacks, leading to enhanced broad-spectrum bactericidal activity. The multidrug-resistant *S. aureus* was inhibited by the ZnO–CuO nanocomposite,

which produced a 24 mm zone of inhibition, whereas ZnO nanoparticles alone produced an 8 mm inhibition zone (Jan *et al.* 2019). Table 3 shows how our research compares to other studies on a number of biological and other applications.

Table 2. Comparative Antibacterial and Antifungal Activities of CuO/ZnO Nanocomposites, CuO Nanoparticles, and Control Treatments

Investigated Microorganisms	Radius of Inhibition Zones (mm)			HSD at 0.05
	CuO/ZnO Nanocomposite	CuO NPs	*Control	
B. subtilis	28 ± 0.1	22 ± 0.1	24 ± 0.1	1.36
S. aureus	25 ± 0.1	15 ± 0.2	16 ± 0.1	1.10
K. pneumoniae	21 ± 0.2	13 ± 0.1	19 ± 0.1	2.32
S. typhi	24 ± 0.2	14 ± 0.2	16 ± 0.1	1.56
C. albicans	29 ± 0.2	24 ± 0.1	22 ± 0.3	1.05
A. terreus	29 ± 0.2	25 ± 0.1	32 ± 0.3	2.36

*Gentamicin (10 µg/mL) or Fluconazole (25 µg/mL) was used as the positive standard in the antibacterial or antifungal assay, respectively

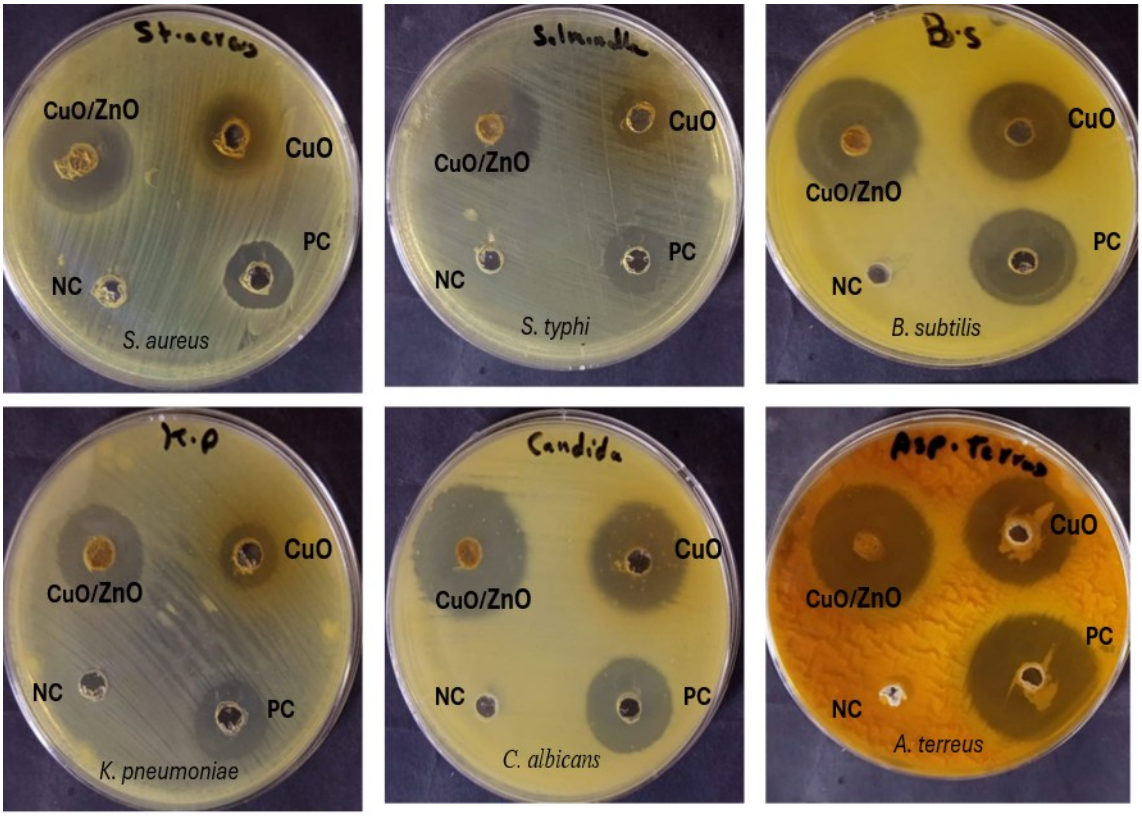

Fig. 5. Agar well diffusion assay showing inhibition zones produced by CuO/ZnO nanocomposites, CuO nanoparticles, and controls against bacterial and fungal pathogens

Table 3. A Comparison of the Present Work with Other Studies Concerning Several Biological and Other Applications of CuO/ZnO NPs

Synthesis means	Biological significance of CuO/ZnO NPs	Reference
Neem plant leaves	Methylene blue degradation	(Gemachu *et al*. 2025)
Wet-chemical synthesis	Dyes degradation	(Mohammed *et al.* 2025)
Urtica urens extract	Antimicrobial and cytotoxicity activity	(Fouda *et al*. 2025)
Co-precipitation method	Antibacterial activity	(Karrari *et al*. 2025)
Co-precipitation method	Antibacterial and antifungal activity	(Aziz *et al*. 2024)
Tribulus terrestris Aqueous Extract	Antibacterial activity	(Kalaiyarasi *et al*. 2025)
Ageratum conyzoides L. leaf extract	Antibacterial, antioxidant agents, and dyes degradation	(Leishangthem *et al.* 2025)
Ultrasound-assisted coprecipitation	As (III) Removal from Water	(Medina Salas *et al* 2023)
Aqueous extract of *Capparis spinosa* L. leaves.	Removal dyes of wastewater	(Khaled et al. 2025)
Synadium grantii leaf extract	Deterioration of dangerous organic contaminants	(Karthik et al. 2022)
Guava Leaf extract	Antimicrobial, antioxidant, and anticancer activities	Current study

Table 4 summarizes the cytotoxic effects of CuO and CuO/ZnO nanoparticles on Wi38 normal fibroblast cells and SKOV3 ovarian cancer cells across a concentration range of 1000 to 31.25 µg/mL. The data demonstrates a concentration-dependent cytotoxic response, where cell viability increased at higher concentrations but declined sharply at lower concentrations. For Wi38 normal cells, CuO showed cytotoxicity at low concentrations, reducing viability to nearly zero at 250 to 31.25 µg/mL. In contrast, CuO/ZnO NPs preserved much higher viability at equivalent doses 49.3% at 250 µg/mL and 0.18% at 62.5 µg/mL, indicating better biocompatibility of the nanocomposite compared to CuO alone. For SKOV3 cancer cells, both nanoparticle types displayed clear antiproliferative activity, but CuO/ZnO NPs exhibited notably stronger anticancer effects. At low concentrations (250, 125, and 62.5 µg/mL), SKOV3 cell viability decreased substantially (87.17%, 79.08%, and 47.42%, respectively), while CuO NPs showed comparatively weaker inhibition. Statistically, CuO/ZnO NPs appeared the highest significant efficiency against SKOV3 cancer cells at low concentration compared to CuO NPs alone. The calculated IC_{50} values further confirm selective toxicity, where it was 397.35 ± 2.76 µg/mL and 295.48 ± 1.93 µg/mL employing CuO NPs and CuO/ZnO NPs, respectively, against Wi38 cell line. Meanwhile, it was 122.25 ± 2.38 µg/mL and 81.87 ± 0.82 µg/mL employing CuO NPs and CuO/ZnO NPs, respectively, against SKOV3 cell line. These values clearly indicate that CuO/ZnO NPs are more cytotoxic to cancer cells than normal cells, highlighting their potential as selective anticancer agents.

This difference may be attributed to differences in cellular metabolism, membrane properties, and redox balance between cancerous and normal cells. Cancer cells typically exhibit higher metabolic activity and a more vulnerable oxidative status, which may enhance their sensitivity to nanoparticle-induced stress.

Figure 6 depicts the morphological changes in Wi38 normal fibroblast cells following exposure to increasing concentrations of CuO (a) and CuO/ZnO NPs (b). Untreated control cells maintained normal spindle-shaped morphology and strong confluence. At low nanoparticle concentrations (31.25 to 125 µg/mL), CuO induced milder cellular shrinkage, membrane damage, and loss of confluence, consistent with the viability drop shown in Table 4. However, Wi38 cells exposed to the nanocomposite (CuO/ZnO) displayed severe alterations, retaining adherence and structural integrity, which supports the lower IC_{50}.

Additionally, Fig. 7 illustrates the dose-dependent morphological responses of SKOV3 cancer cells to CuO (a) and CuO/ZnO NPs (b). Control cells exhibited typical epithelial-like morphology with dense, well-defined colonies. Upon treatment with low to moderate nanoparticle concentrations (31.25 to 250 µg/mL), SKOV3 cells underwent marked morphological deterioration, including rounding, detachment, cytoplasmic condensation, and reduced cell density. These changes were more pronounced in the CuO/ZnO nanoparticle group, consistent with their stronger cytotoxic effect. The observed cytotoxic effects of CuO and CuO/ZnO NPs can be explained *via* induction of ROS generation as a probable mechanism, membrane disruption, and/or nanoparticle–cell interactions. In addition, several studies have highlighted the enhanced anticancer potential of CuO-ZnO nanoparticles. For instance, CuO–ZnO NPs demonstrated significant cytotoxicity against the MCF7 human breast cancer cell line, with an IC50 of 239.99 µg/mL (Daimari and Deka 2024). Similarly, hexagonal ZnO-CuO biphasic nanoparticles synthesized using *Sambucus nigra* L. extract exhibited notable anticancer effects against lung and melanoma cancer cells (Cao *et al.* 2021). Moreover, spherical ZnO-CuO biphasic nanoparticles produced *via* green synthesis were reported to possess both strong antibacterial properties and potent anticancer activity against MCF-7 cells (Madeshwaran and Venkatachalam 2024). These results suggest that combining ZnO and CuO in nanoparticle form can improve anticancer properties, making them promising candidates for biomedical applications.

Table 4. Cytotoxicity % of CuO and CuO/ZnO NPs against Wi38 and SKOV3 Cell Lines

Concentration (µg/mL)	Wi38		SKOV3		HSD at 0.05
	CuO NPs	synergistic	CuO NPs	CuO/ZnO NPs	
1000	96.93 ± 0.65	97.02 ± 0.54	93.49 ± 0.45	94.62 ± 0.65	0.02
500	74.11 ± 1.32	97.07 ± 0.45	89.97 ± 0.36	91.14 ± 0.36	0.25
250	0.96 ± 0.10	49.33 ± 1.02	89.06 ± 1.21	87.17 ± 0.45	3.36
125	0.64 ± 0.08	0.64 ± 0.04	52.34 ± 0.65	79.08 ± 1.16	2.35
62.5	0.0 ± 0.0	0.18 ± 0.06	12.64 ± 0.25	47.42 ± 0.08	4.36
31.25	0.0 ± 0.0	0.0 ± 0.0	0.27 ± 0.01	0.0 ± 0.0	0.06
IC_{50} (µg/mL)	397.35 ± 2.76	295.48 ± 1.93	122.25 ± 2.38	81.87 ± 0.82	5.36

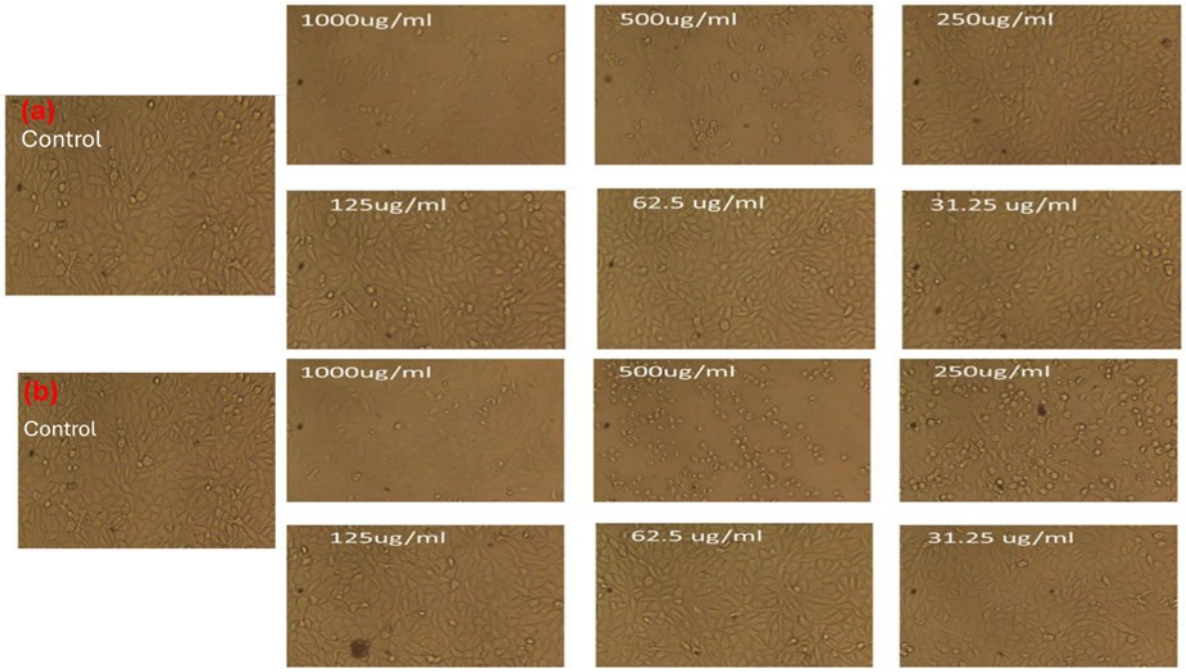

Fig. 6. Morphological changes of Wi38 cell lines in response to CuO (a) and CuO/ZnO NPs (b)

The antioxidant capacity was determined using the DPPH free-radical scavenging assay for ascorbic acid, CuO NPs, and CuO/ZnO nanocomposites, in the concentration range of 0 to 1000 µg/mL. All three samples showed dose-dependent results. At low doses of 1.95 to 7.81 µg/mL, standard ascorbic acid had an inhibitory range of 41.0 to 57.0%, CuO/ZnO nanocomposite (33.6 to 50.8%) showed a highly significant scavenging ability than CuO NPs (27.5 to 45.3%) (Table 5). At 125 µg/mL, the nanocomposite had 84.2% scavenging ability, which was better than pure CuO (79.8%), while CuO was less active than ascorbic acid (86.4%) (Table 5). The nanocomposite (93.7 to 95.7%) still had a better scavenging capacity than CuO NPs (90.2 to 93.7%) at high concentrations of 500 to 1000 µg/mL. IC_{50} values of ascorbic acid, CuO/ZnO, and CuO were calculated as 3.61 ± 0.06, 6.93 ± 0.25, and 11.61 ± 0.33 µg/mL, respectively. Among all the samples, ascorbic acid showed the highest activity, which was followed by the CuO/ZnO composite and CuO NPs (Table 5). The observed greater activity of the nanocomposite is attributed to the combination interfacial effect. The reactivity of the nanocomposite was increased due to the introduction of ZnO, which enhanced the number of active sites and improved the transfer of electrons (Afifi *et al.* 2015).

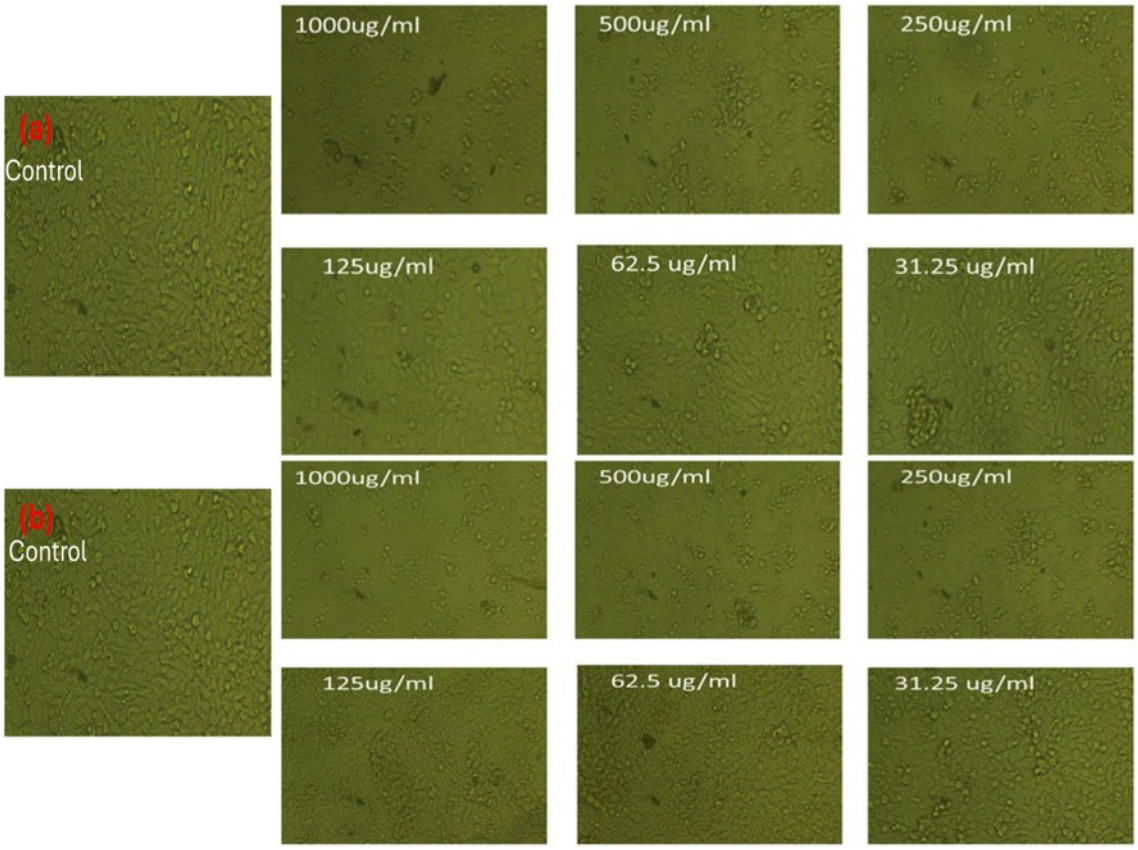

Fig. 7. Morphological changes of SKOV3 cancer cell lines in response to CuO (a) and CuO/ZnO NPs (b)

The present results are also in line with recent studies (Daimari and Deka 2024; Azabi *et al.* 2025). The radicals are more stabilized in the heterojunction than in individual oxides. Thus, CuO/ZnO nanocomposites are expected to be applied in various fields for the scavenging of free radicals and oxidative stress, which include pharmaceutical, cosmetic, and food-preservation industries.

Table 5. Antioxidant Effect *via* DPPH Scavenging at Different Concentration of CuO and CuO/ZnO NPs Compared with Standard Compounds

Concentration (µg/mL)	Antioxidant *via* DPPH Scavenging (%)			HSD at 0.05
	Ascorbic Acid	CuO NPs	CuO/ZnO NPs	
0.0	0.0	0.0	0.0	0.00
1.95	41.0±0.65	27.5±0.48	33.6±1.21	3.25
3.9	50.3±1.02	36.4±0.85	42.7±0.46	2.65
7.81	57.0±0.45	45.3±0.49	50.8±0.80	4.36
15.62	64.2±0.74	54.3±0.36	58.6±0.46	2.49
31.25	72.8±0.49	62.6±0.68	67.7±0.28	3.84
62.5	79.3±1.21	72.2±0.34	76.7±1.03	2.19
125	86.4±0.25	79.8±0.59	84.2±0.42	3.36
250	92.3±0.42	84.8±0.24	90.7±0.38	2.68
500	95.4±0.59	90.2±0.82	93.7±0.47	2.98
1000	98.2±0.87	93.7±0.19	95.7±0.35	3.98
IC_{50} µg/mL	3.61 ± 0.06	11.61 ± 0.33	6.93 ± 0.25	2.74

CONCLUSIONS

1. Monophasic nanoparticles of Cu and biphasic nanoparticles of Cu/Zn oxide were prepared *via* green synthesis and characterized by X-ray diffraction (XRD), Fourier transform infrared (FTIR) spectroscopy, and transmission electron microscopy (TEM), which verified that ZnO and CuO formation.
2. The CuO/ZnO nanocomposite displayed potent antioxidant activity, indicating a strong combination effect between CuO and ZnO.
3. *P. guajava*-derived CuO/ZnO nanocomposite presents a promising multifunctional material with potential applications in antimicrobial therapies, antioxidant formulations, and anticancer strategies.

FUNDING

This work was supported and funded by the Deanship of Scientific Research at Imam Mohammad Ibn Saud Islamic University (IMSIU) (grant number IMSIU-DDRSP2601)

REFERENCES CITED

Abd-ElGawad, A. M., Amin, M. A., Ismail, M. A., Ismail, M. K., Radwan, A. A., Sarker, T. C., El-Naggar, M. A., and Abdelkareem, E. M. (2025). "Selenium/copper oxide nanoparticles prepared with *Urtica urens* extract: Their antimicrobial, antioxidant, antihemolytic, anticoagulant, and plant growth effects," *BioResources* 20(2), 2791-2810. https://doi.org/10.15376/biores.20.2.2791-2810

Abdelghany, T. A., Bakri, M. M., Al-Rajhi, A. M., Al Abboud, M. A., Alawlaqi, M. M., and Shater, A. R. M. (2020). "Impact of copper and its nanoparticles on growth, ultra-structure, and laccase production of *Aspergillus niger* using corn cobs wastes," *BioResources* 15(2), 3289-3306. https://doi.org/10.15376/biores.15.2.3289-3306

Abdelghany, T. M., Al-Rajhi, A. M. H., Al Abboud, M. A., Alawlaqi, M. M., Magdah, A. G., Helmy, E. A. M., and Mabrouk, A. S. (2018). "Recent advances in green synthesis of silver nanoparticles and their applications: About future directions. A review," *BioNanoScience* 8(1), 5-16. https://doi.org/10.1007/s12668-017-0413-3

Abdelghany, T. M., Al-Rajhi, A. M., Almuhayawi, M. S., Abada, E., Al Abboud, M. A., Moawad, H., and Selim, S. (2023a). "Green fabrication of nanocomposite doped with selenium nanoparticle–based starch and glycogen with its therapeutic activity: Antimicrobial, antioxidant, and anti-inflammatory *in vitro*," *Biomass Conversion and Biorefinery* 13(1), 431-443. https://doi.org/10.1007/s13399-022-03257-8

Abdelghany, T. M., Al-Rajhi, A. M. H., Yahya, R., Bakri, M. M., Al Abboud, M. A., Yahya, R., and Salem, S. S. (2023b). "Phytofabrication of zinc oxide nanoparticles with advanced characterization and its antioxidant, anticancer, and antimicrobial activity against pathogenic microorganisms," *Biomass Conv. Bioref.* 13, 417-430. https://doi.org/10.1007/s13399-022-03412-1

Abdelhady, M. A., Abdelghany, T. M., Mohamed, S. H., and Abdelbary, S. A. (2024). "Impact of green synthesized zinc oxide nanoparticles for treating dry rot in potato

tubers," *BioResources* 19(2), 2106-2119. https://doi.org/10.15376/biores.19.2.2106-2119

Afifi, M., Almaghrabi, O. A., and Kadasa, N. M. (2015). "Ameliorative effect of zinc oxide nanoparticles on antioxidants and sperm characteristics in streptozotocin-induced diabetic rat testes," *Biomed. Res. Int.* 2015, article 153573. https://doi.org/10.1155/2015/153573

Al Abboud, M. A., Mashraqi, A., Qanash, H., Gattan, H. S., Felemban, H. R., Alkorbi, F., and Moawad, H. (2024). "Green biosynthesis of bimetallic ZnO@AuNPs with its formulation into cellulose derivative: Biological and environmental applications," *Bioresour. Bioprocess.* 11, article 60. https://doi.org/10.1186/s40643-024-00759-3

Alawlaqi, M. M., Al-Rajhi, A. M. H., Abdelghany, T. M., Ganash, M., and Moawad, H. (2023). "Evaluation of biomedical applications for linseed extract: Antimicrobial, antioxidant, anti-diabetic, and anti-inflammatory activities *in vitro*," *Journal of Functional Biomaterials* 14(6), article 300. https://doi.org/10.3390/jfb14060300

Alghonaim, M. I., Alsalamah, S. A., Mohammad, A. M. and Abdelghany, T. M. (2025). "Green synthesis of bimetallic Se@TiO_2NPs and their formulation into biopolymers and their utilization as antimicrobial, anti-diabetic, antioxidant, and healing agent *in vitro*," *Biomass Conv. Bioref.* 15, 6767-6779. https://doi.org/10.1007/s13399-024-05451-2

Al-Rajhi, A. M. H., Yahya, R., Alawlaqi, M. M., Fareid, M. A., Amin, B. H., and Abdelghany, T. M. (2022). "Copper oxide nanoparticles as fungistat to inhibit mycotoxins and hydrolytic enzyme production by *Fusarium incarnatum* isolated from garlic biomass," *BioResources* 17(2), 3042-3056. https://doi.org/10.15376/biores.17.2.3042-3056

Alsalamah, S. A., Alghonaim, M. I., Bakri, M. M., and Abdelghany, T. M. (2024). "*Zygnema* sp. as creator of copper oxide nanoparticles and their application in controlling of microbial growth and photo-catalytic degradation of dyes," *Appl. Biol. Chem.* 67(1), article 47. https://doi.org/10.1186/s13765-024-00891-w

Amin, M. A. A., Abu-Elsaoud, A. M., Nowwar, A. I., Abdelwahab, A. T., Awad, M. A., Hassan, S. E. D., and Elkelish, A. (2024). "Green synthesis of magnesium oxide nanoparticles using endophytic fungal strain to improve the growth, metabolic activities, yield traits, and phenolic compounds content of *Nigella sativa* L," *Green Process. Syn.* 13(1), article 20230215. https://doi.org/10.1515/gps-2023-0215

Amin, M. A., Algamdi, N. A., Waznah, M. S., Bukhari, D. A., Alsharif, S. M., Alkhayri, F., Abdel-Nasser, M. and Fouda, A. (2025). "An insight into antimicrobial, antioxidant, anticancer, and antidiabetic activities of trimetallic Se/ZnO/CuO nanoalloys fabricated by aqueous extract of *Nitraria retusa*," *J. Cluster Sci.* 36(1), 1-15. https://doi.org/10.1007/s10876-024-02742-6

Atiek, E., Matebu, A., Tsegaye, D., Behailu, G., and Abebe, B. (2024). "Green synthesis of TiO_2/ZnO heterostructure using *Urtica Smensis* leaf extract for antibacterial activity," *Results in Chemistry* 12, article 101880. https://doi.org/10.1016/j.rechem.2024.101880

Azabi, W., Gherraf, N., Romero, A., and Abdullah, J. A. A. (2025). "Synergetic green synthesis of CuO, ZnO, and CuO-ZnO nanocomposite nanoparticles using *Genista hispanica* L. extract for enhanced photocatalytic and antioxidant properties," *Res. Chem. Intermed.* 51, 4491-4517. https://doi.org/10.1007/s11164-025-05663-9

Aziz, S. N., Abdulwahab, A. M., Aldeen, T. S., and Alqabili, D. M. A. (2024). "Synthesis, characterization, and evaluation of antibacterial and antifungal activities of CuO-ZnO-Co_3O_4 nanocomposites," *Heliyon* 10(18). https://doi.org/10.1016/j.heliyon.2024.e37802

Bashiri, M., Rezanezhad, M., Tavakkoli-Moghaddam, R., and Hasanzadeh, H. (2018). "Mathematical modeling for a p -mobile hub location problem in a dynamic environment by a genetic algorithm," *Appl. Math. Mod.* 54, 151-169. https://doi.org/10.1016/j.apm.2017.09.032

Cao, Y., Dhahad, H. A., El-Shorbagy, M. A., Alijani, H. Q., Zakeri, M., Heydari, A., Bahonar, E., Slouf, M., Khatami, M., Naderifar, M., *et al.* (2021). "Green synthesis of bimetallic ZnO-CuO nanoparticles and their cytotoxicity properties," *Sci. Rep.* 11(1), article 23479. https://doi.org/10.1038/s41598-021-02937-1

Daimari, J., and Deka, A. K. (2024). "Anticancer, antimicrobial and antioxidant activity of CuO–ZnO bimetallic nanoparticles: Green synthesised from *Eryngium foetidum* leaf extract," *Sci. Rep.* 14, article 19506 https://doi.org/10.1038/s41598-024-69847-w

Das, S., and Srivastava, V. C. (2018). "An overview of the synthesis of CuO-ZnO nanocomposite for environmental and other applications," *Nanotechnol. Rev.* 7(3), 267-282. https://doi.org/10.1515/ntrev-2017-0144

Devi, G. K., Kumar, K. S., Parthiban, R., and Kalishwaralal, K. (2016). "An insight study on HPTLC fingerprinting of *Mukia maderaspatna*: Mechanism of bioactive constituents in metal nanoparticle synthesis and its activity against human pathogens," *Microb. Path.* 102, 120-132. https://doi.org/10.1016/j.micpath.2016.11.026

El-Batal, A. I., Ismail, M. A., Amin, M. A., El-Sayyad, G. S., and Osman, M. S. (2023). "Selenium nanoparticles induce growth and physiological tolerance of waste-water-stressed carrot plants," *Biologia* 78(9), 2339-2355. https://doi.org/10.1007/s11756-023-01401-x

Fani, F., Talebpour, C., Leprohon, P., Salimnia, H., Alamdari, H., and Ouellette, M. (2025). "Mode of action of silver-based perovskite against Gram-negative bacteria," *Microbiol Spectr* 13, article e01648-24. https://doi.org/10.1128/spectrum.01648-24

Fouda, A., Alsharif, S. M., Eid, A. M., Albalawi, A. S., Amin, M. A., Alraddadi, F. A., Almutrafy, A.M., Bukhari, D.A., Algamdi, N.A., and Abdel-Rahman, M. A. (2025). "Photocatalytic activity of green-synthesized semiconductor CuO/ZnO nanocomposites against organic dye: An assessment of antimicrobial and cytotoxicity investigations," *Catalysts*, *15*(12), 1096.

Gemachu, L. Y., Terefa, F. H., Berhanu, A. L., and Bogale, R. F. (2025). "Comparison of sunlight-driven photocatalytic activity of eco-friendly synthesized ZnO/CuO, ZnO/NiO and NiO/CuO binary nanocomposites," *Results in Chemistry* 2025, article 102708. https://doi.org/10.1016/j.rechem.2025.102708

Hamed, R., Obeid, R. and Abu-Huwaij, R. (2023). "Plant mediated-green synthesis of zinc oxide nanoparticles: An insight into biomedical applications," *Nanotechnology Reviews*, 12(1), 20230112. https://doi.org/10.1515/ntrev-2023-0112

Jan, T., Azmat, S., Mansoor, Q., Waqas, H. M., Adil, M., Ilyas, S. Z., Ishaq Ahmad, I., and Ismail, M. (2019). "Superior antibacterial activity of ZnO-CuO nanocomposite synthesized by a chemical Co-precipitation approach," *Microb. Path.* 134, article 103579. https://doi.org/10.1016/j.micpath.2019.103579

Kalaiyarasi, M., Mani, M., Harikrishnan, R., Bharathiraja, N., Kishorkumar, J., Sibali, L., and Kaviyarasu, K. (2025). "Study of Zn-Astrakanite/CuO/ZnO nanocomposite using *Tribulus terrestris* aqueous extract, and their structural, optical, morphological, dielectric, and bacterial properties," *Microscopy Research and Technique* 88(12), 3226-3238. https://doi.org/10.1002/jemt.70041

Karrari, S., Mohammadzadeh, H., and Jafari, R. (2025). "Characterization of ZnO-CuO and ZnO-CuO-NiO nanocomposites prepared by co-precipitation and antibacterial properties," *Applied Physics A* 131(2), article 147. https://doi.org/10.1007/s00339-025-08273-9

Karthik, K. V., Raghu, A. V., Reddy, K. R., Ravishankar, R., Sangeeta, M., Shetti, N. P., and Reddy, C. V. (2022). "Green synthesis of Cu-doped ZnO nanoparticles and its application for the photocatalytic degradation of hazardous organic pollutants," *Chemosphere* 287, article 132081. https://doi.org/10.1016/j.chemosphere.2021.132081

Khaled, I. M., Umair, M., Pecoraro, C. M., Kheniche, A., Bellardita, M., and Soltani, S. (2025). "Green synthesis of ZnO and CuO nanoparticles and ZnO-CuO nanocomposites: Characterization and photocatalytic dyes removal efficiency's determination," *Colloids and Surfaces A: Physicochemical and Engineering Aspects* 2025, article 138544. https://doi.org/10.1016/j.colsurfa.2025.138544

Leishangthem, N., Singh, T. S., and Singh, N. M. (2025). "Green synthesis of CuO/ZnO/g-C_3N_4 and ZnO/g-C_3N_4 nanocomposites using *Ageratum conyzoides* L. leaf extract: Multifunctional applications in dye degradation, antimicrobial, antioxidant, and phytotoxic activities," *Inorganic Chemistry Communications*, 2025, article 115048. https://doi.org/10.1016/j.inoche.2025.115048

López-López, J., Tejeda-Ochoa, A., López-Beltrán, A., Herrera-Ramírez, J., and Méndez-Herrera, P. (2021). "Sunlight photocatalytic performance of ZnO nanoparticles synthesized by green chemistry using different botanical extracts and zinc acetate as a precursor," *Molecules*, *27*(1), 6. https://doi.org/10.3390/molecules27010006

Ma, N., Wang, Y., Li, X., Xu, M., and Tan, D. (2025). "Reactive oxygen species in cancer: Mechanistic insights and therapeutic innovations," *Cell Stress Chaperones* 30(5), article 100108. https://doi.org/10.1016/j.cstres.2025.100108.

Madeshwaran, K. and Venkatachalam, R. (2024). "Green synthesis of bimetallic ZnO–CuO nanoparticles using *Annona muricata* l. extract: Investigation of antimicrobial, antioxidant, and anticancer properties," *J. Ind. Eng. Chem.* 140, 454-467. https://doi.org/10.1016/j.jiec.2024.06.002

Matinise, N., Fuku, X. G., Kaviyarasu, K., Mayedwa, N., and Maaza, M. J. (2017). "ZnO nanoparticles via Moringa oleifera green synthesis: Physical properties & mechanism of formation," *Applied surface science*, 406, 339-347. https://doi.org/10.1016/j.apsusc.2017.01.219

Medina Salas, J. P., Gamarra Gómez, F., Sacari Sacari, E. J., Lanchipa Ramos, W. O., Tamayo Calderón, R. M., Mamani Flores, E., ... and Sandoval, E. M. L. (2023). "ZnO-CuO nanocomposite as an efficient adsorbent for As (III) removal from water," *Water* 15(24), article 4318. https://doi.org/10.3390/w15244318

Mohammed, S. O., Khalil, M. M., El-Sewify, I. M., and Radwan, A. (2025). "Nd-doped CuO/ZnO and ZnO/CuO heterojunctions for simultaneous UV blocking and malachite green detoxification," *Scientific Reports* 15(1), 1-21. https://doi.org/10.1038/s41598-025-13945-w

Music, S., Popović, S., Maljković, M., and Dragčević, Đ. (2002). "Influence of synthesis procedure on the formation and properties of zinc oxide," *Journal of Alloys and Compounds* 347(1-2), 324-332. https://doi.org/10.1016/S0925-8388(02)00792-2

Nguyen, N. H., Padil, V. V. T., Slaveykova, V. I., Černík, M., and Ševců, A. (2018). "Green synthesis of metal and metal oxide nanoparticles and their effect on the unicellular alga *Chlamydomonas reinhardtii*," *Nanos. Res. Lett.* 13(1), article 159.

Park, H., Kim, B., Kang, Y., and Kim, W. (2024). "Study on chemical composition and biological activity of *Psidium guajava* leaf extracts," *Curr. Issue. Mol. Biol.* 46(3), 2133-2143. https://doi.org/10.3390/cimb46030137

Qanash, H., Al-Rajhi, A. M., Almashjary, M. N., Basabrain, A. A., Hazzazi, M. S., and Abdelghany, T. M. (2023). "Inhibitory potential of rutin and rutin nano-crystals against *Helicobacter pylori*, colon cancer, hemolysis and butyrylcholinesterase *in vitro* and *in silico*," *Appl. Biol. Chem.* 66(1), article 79. https://doi.org/10.1186/s13765-023-00832-z

Qanash, H., Bazaid, A. S., Alharazi, T., Barnawi, H., Alotaibi, K., Shater, A. R. M., and Abdelghany, T. M. (2024). "Bioenvironmental applications of myco-created bioactive zinc oxide nanoparticle-doped selenium oxide nanoparticles," *Biomass Conv. Bioref.* 14(15), 17341-17352. https://doi.org/10.1007/s13399-023-03809-6

Selim, S., Abdelghany, T. M., Almuhayawi, M. S., Nagshabandi, M. K., Tarabulsi, M. K., Elamir, M. Y. M., Alharbi, A.A., and Al Jaouni, S. K. (2025a). "Biosynthesis and activity of Zn-MnO nanocomposite in vitro with molecular docking studies against multidrug resistance bacteria and inflammatory activators," *Scientific Reports* 15(1), article 2032. https://doi.org/10.1038/s41598-024-85005-8

Selim, S., Saddiq, A. A., Ashy, R. A., Baghdadi, A. M., Alzahrani, A. J., Mostafa, E. M., Al Jaouni, S. K., Elamir, M. Y. M., Amin, M. A., Salah, A. M., *et al.* (2025b). "Bimetallic selenium/zinc oxide nanoparticles: Biological activity and plant biostimulant properties," *AMB Express* 15(1), 1-11. https://doi.org/10.1186/s13568-024-01808-y

Senthilkumaar, S., K. Rajendran, S. Banerjee, T. K. Chini, and V. Sengodan (2008). "Influence of Mn doping on the microstructure and optical property of ZnO," *Mater. Sci. Semiconduct. Process.* 11, 6-12. https://doi.org/10.1016/j.mssp.2008.04.005

Turabik, M., Özdemir, S., Akinbingol, G., Gonca, S., and Gecgel, C. (2023). "Comparison of antioxidant, antimicrobial, DNA cleavage, cell viability, and biofilm inhibition activities of mono- and bimetallic copper and zinc nanoparticles," *Inorgan. Chem. Commun.* 155, article 111072. https://doi.org/10.1016/j.inoche.2023.111072

Vishveshvar, K., Aravind Krishnan, M. V., Haribabu, K., and Vishnuprasad, S. (2018). "Green synthesis of copper oxide nanoparticles using *Ixiro coccinea* plant leaves and its characterization," *BioNanoSci.* 8 (2), 554-558. https://doi.org/10.1007/s12668-018-0508-5

Yallappa, S., Manjanna, J., Sindhe, M. A., Satyanarayan, N. D., Pramod, S. N., and Nagaraja, K. (2013). "Microwave assisted rapid synthesis and biological evaluation of stable copper nanoparticles using *T. arjuna* bark extract," *Spectr. Acta Part A: Mol. Biomol. Spect.* 110, 108-115. https://doi.org/10.1016/j.saa.2013.03.005

Article submitted: November 26, 2025; Peer review completed: January 17, 2026; Revised version received: January 19, 2026; Further revised version received and accepted: January 21, 2026; Published: February 5, 2026.
DOI: 10.15376/biores.21.2.2906-2924